Quantum molecular dynamics study of the mass distribution of products in 7.0*A* MeV ^{238}U + ^{238}U collisions

Kai Zhao,[1] Xizhen Wu,[1,*] and Zhuxia Li[1,2,†]

[1]*China Institute of Atomic Energy, Post Office Box 275(18), Beijing 102413, People's Republic of China*

[2]*Institute of Theoretical Physics, Chinese Academy of Science, Beijing 100080, People's Republic of China*

(Received 21 September 2009; published 18 November 2009)

Within the improved quantum molecular dynamics (ImQMD) model incorporating the statistical decay model, the reactions of ^{238}U + ^{238}U at an energy of 7.0*A* MeV have been studied. The charge, mass, and excitation energy distributions of primary fragments are investigated within the ImQMD model, and de-excitation processes of these primary fragments are described by a statistical decay model. The mass distribution of the final products in ^{238}U + ^{238}U collisions is obtained and compared with the recently obtained experimental data.

DOI: 10.1103/PhysRevC.80.054607 PACS number(s): 25.70.Lm, 25.70.Jj

I. INTRODUCTION

When beams in the actinide region with bombarding energies above the Coulomb barrier became available about twenty years ago, the strongly damped reactions in very heavy systems, such as in ^{238}U + ^{238}U, were studied [1–3]. The focus of these early experiments was to investigate the decay channels of the dinuclear system (for production of superheavy nuclei) or particle creation in strong electromagnetic fields. Recently, renewed interest in this subject has been generated by the need to clarify the dynamics of very heavy nuclear collisions at low excitation energies and by the search for new ways of producing neutron-rich superheavy nuclei. On the basis of coupled Langevin-type equations, a model for the simultaneous description of deep inelastic scattering, quasifission, fusion, and regular fission was proposed in Ref. [4]. Within this model, the reactions of ^{238}U + ^{238}U, ^{232}Th + ^{250}Cf, and ^{238}U + ^{248}Cm were investigated and large transfers of charge and mass were found as a result of an inverse quasifission process [4,5]. Owing to very heavy nuclear system and very complicated process, a large number of degrees of freedom, such as those in the excitation and deformation of projectile and target, neck formation, nucleon transfer, different types of separation of the composite system, and nucleon emission will simultaneously play a role. Thus, it is difficult to handle problems with such a complex mechanism and a large number of degrees of freedom by a macroscopic dynamics model. In this case, a microscopic transport theory model is appropriate [6,7]. In Ref. [7], the formation and properties of the transiently formed composite systems in strongly damped reactions of ^{238}U + ^{238}U and ^{232}Th + ^{250}Cf at $E_{\rm cm}$ = 680–1880 MeV were studied on the basis of the improved quantum molecular dynamics (ImQMD) model. It was found that the weakly repulsive entrance channel potential and the strong dissipation delay the reseparation time of a composite system, and a 15–20-MeV-high Coulomb barrier at the surface of the single-particle potential well of the composite system makes the excited unbound protons remain embedded in the potential well and move in a common mono-single-particle potential for a period of time. These two effects restrain the quick decay of the composite system. The findings of this previous study generated our interest in the incident-energy dependence of lifetime of the composite system. We found that the longest average lifetime for the composite system of ^{238}U + ^{238}U could reach over ∼1000 fm/c at an incident energy region of 1000–1300 MeV. Recent study of the incident-energy dependence of the lifetime of the transiently formed giant composite system ^{238}U + ^{238}U using time-dependent Hartree-Fock (TDHF) calculations based on the Skyrme energy density functional [8] confirmed this result. Since the correlation (fluctuation) effect is considered in the ImQMD model, it enables calculation of the mass (charge) distribution of primary fragments in the ^{238}U + ^{238}U reaction, in addition to study of the properties of the composite systems. The experiment for the reaction ^{238}U + ^{238}U at energies close to the Coulomb barrier was performed at GANIL, and the mass distributions of products of the reaction at several energies are now available [9,10], which encouraged us to undertake further study of the decay of the composite system of ^{238}U + ^{238}U.

In this work, we study the mass distribution of products in ^{238}U + ^{238}U at 7*A* MeV, and then compare it with the experimental data. Considering the extreme complexity of the reaction process and the need to reduce computation time, we describe the reaction process by a two-step model, that is, a dynamical reaction process described by the ImQMD model followed by a statistical decay process, which is described by a statistical decay model.

The paper is organized as follows: In Sec. II, we briefly introduce the theoretical models. In Secs. III and IV, we present the results of primary fragments and final products, respectively. Finally, we give a brief summary in Sec. V.

II. THEORETICAL MODEL

In this approach, the first step describes the formation and reseparation of the transiently formed composite systems of ^{238}U + ^{238}U using the ImQMD model. The primary fragments

*lizwux9@ciae.ac.cn

†lizwux@ciae.ac.cn

and fast particle emission are obtained at the end of the ImQMD calculations. The second step is devoted to describing the decay of the primary fragments using the computer code HIVAP incorporating a three-Gaussian model to describe the mass distribution of fission fragments. Finally, the mass distribution of the products is obtained.

A. The ImQMD model

A detailed description of the ImQMD model and its applications in low-energy heavy-ion collisions can be found in Refs. [6,7,11,12]. Here, we only mention that, in this model, the nuclear potential energy is an integration of the potential energy density functional, which reads

$$V_{\rm loc} = \frac{\alpha}{2}\frac{\rho^2}{\rho_0} + \frac{\beta}{\gamma+1}\frac{\rho^{\gamma+1}}{\rho_0^{\gamma}} + \frac{g_0}{2\rho_0}(\nabla\rho)^2 + \frac{c_s}{2\rho_0}[\rho^2 - \kappa_s(\nabla\rho)^2]\delta^2 + g_\tau\frac{\rho^{\eta+1}}{\rho_0^{\eta}}, \quad (1)$$

where ρ, ρ_n, and ρ_p are the nucleon, neutron, and proton densities, and $\delta = (\rho_n - \rho_p)/(\rho_n + \rho_p)$ is the isospin asymmetry. The parameters in these expressions are given in Table I [6].

The Coulomb energy is also included in the Hamiltonian, written as the sum of the direct and the exchange contributions:

$$U_{\rm Coul} = \frac{1}{2}\iint \rho_p(\mathbf{r})\frac{e^2}{|\mathbf{r}-\mathbf{r}'|}\rho_p(\mathbf{r}')d\mathbf{r}\,d\mathbf{r}' - e^2\frac{3}{4}\left(\frac{3}{\pi}\right)^{1/3}\int \rho_p^{4/3}d\mathbf{R}. \quad (2)$$

In the collision term, isospin-dependent nucleon-nucleon scattering cross sections [13] are used and the Pauli blocking effect is treated more strictly [14,15].

It is critical that the initial nuclei are set in the real ground state because considerable excitation of initial nuclei will produce unreal particle emission and a residue with an excitation that is too high, which will completely mask the real decay process of the residue. We carefully check not only the binding energy and the root-mean-square radius of the initial nuclei but also their time evolution. The average binding energy per nucleon of initial nuclei is required to be $E_{\rm gs} \pm 0.1$ MeV, where $E_{\rm gs}$ is the binding energy of nuclei in the ground state. It is necessary that the initial nuclei with no spurious particle emission and their properties, such as the binding energy and root-mean-square radius being stable within 6000 fm/c, are taken to be those of good initial nuclei and are then applied in the simulation of the reaction process. The deformation of the initial ^{238}U ($\varepsilon = 0.24$) is considered in the initial condition. In the simulation of reactions, the initial orientations of two deformed ^{238}U are randomly taken.

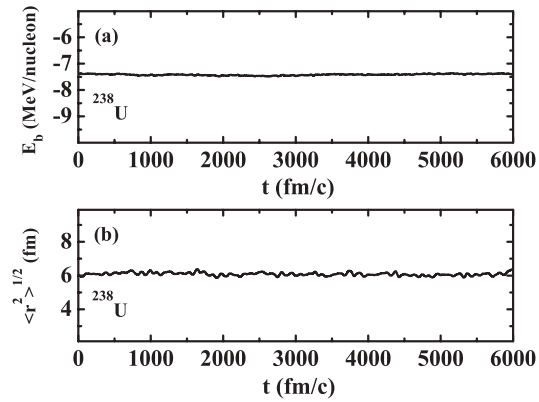

FIG. 1. The time evolution of (a) the binding energy and (b) the root-mean-square radius of the initial ^{238}U.

Figure 1 shows the time evolution of the binding energy and root-mean-square radius of the initial ^{238}U.

At the end of the ImQMD calculations, fragments are constructed using the coalescence model widely used in the QMD calculations. In this work, only the primary fragments with a mass number larger than 50 are considered. Then, we calculate the total energy of each excited fragment in its rest frame, and its excitation energy is obtained by subtracting the corresponding ground-state energy from the total energy of the excited fragment.

B. The statistical decay model

The second step describes the decay process of primary fragments by the emission of neutrons, protons, and α particles, as well as fission. The statistical decay model (HIVAP code) [16] incorporating a three-Gaussian model for the mass distribution of fission fragments for fissile nuclei is used to describe the decay process of primary fragments and the mass distribution of final products. In HIVAP, the survival probability of an excited primary fragment is given by a subsequent de-excitation process, leading to a given final evaporation-residue nucleus in its ground state. Successive stages of a subsequent de-excitation process for primary fragments with mass A, charge Z, and excitation energy E are determined by branching ratios expressed by relative partial decay widths for all possible decay modes, $\Gamma_i(A,Z,E)/\Gamma_{\rm tot}(A,Z,E)$, where $i = n, p, d, \alpha$, etc. and $\Gamma_{\rm tot}(A,Z,E)$ is the sum of all particle decay widths $\Gamma_i(A,Z,E)$ and the fission width $\Gamma_f(A,Z,E)$. All partial widths for emission of light particles and fission for excited nuclei are calculated by the HIVAP code.

The excited actinide and transactinide nuclei in primary fragments and those produced in the de-excitation process undergo fission. The production probability of a fission

TABLE I. The model parameters.

α (MeV)	β (MeV)	γ	g_0 (MeV fm^2)	g_τ (MeV)	η	c_s (MeV)	κ_s (fm^2)	ρ_0 (fm^{-3})
−356	303	7/6	7.0	12.5	2/3	32	0.08	0.165

fragment with mass number A_1 is calculated as follows:

$$W_f(A_1) = \sum_{A,Z,E} \frac{\Gamma_f(A,Z,E)}{\Gamma_{\rm tot}(A,Z,E)} P(A_1,A,Z,E). \quad (3)$$

Here, $P(A_1, A, Z, E)$ is the probability of production of a fragment with mass number A_1 from fission of the excited nucleus with mass A, charge Z, and excitation energy E. $P(A_1, A, Z, E)$ is calculated on the basis of an empirical three-Gaussian model and is given as

$$P(A_1,A,Z,E) = \sum_{j=1}^{3} g^{(j)}(A_1,A,Z,E) \quad (4)$$

and

$$g^{(j)}(A_1,A,Z,E) = \frac{P^{(j)}(A,Z,E)}{\sqrt{2\pi}\sigma^{(j)}(A,Z,E)} \times \exp\left\{-\frac{[A_1 - A^{(j)}(A,Z,E)]^2}{2[\sigma^{(j)}(A,Z,E)]^2}\right\}, \quad j = 1,2,3. \quad (5)$$

Here, the Gaussian distribution $g^{(j)}(A_1, A, Z, E)$ represents one of the components of the mass distribution of fission. Among them, $g^{(1)}(A_1, A, Z, E)$ and $g^{(2)}(A_1, A, Z, E)$ describe the asymmetric component of the mass distribution, and $g^{(3)}(A_1, A, Z, E)$ describes the symmetric component. $P^{(j)}(A, Z, E)$, $\sigma^{(j)}(A, Z, E)$, and $A^{(j)}(A, Z, E)$ are the parameters for three-Gaussian distributions, which are functions of the mass number A, charge Z, and excitation energy E of the fissile nucleus. $P^{(j)}(A, Z, E)$ and $A^{(j)}(A, Z, E)$ exhibit the following relationships:

$$P^{(1)}(A,Z,E) = [1 - P^{(3)}(A,Z,E)]\eta, \quad (6)$$

$$P^{(2)}(A,Z,E) = [1 - P^{(3)}(A,Z,E)](1-\eta), \quad (7)$$

$$A^{(1)}(A,Z,E) + A^{(2)}(A,Z,E) = A, \quad (8)$$

$$A^{(3)}(A,Z,E) = \frac{A}{2}. \quad (9)$$

Thus, only six parameters of $P^{(3)}(A, Z, E)$, η, $A^{(1)}(A, Z, E)$, and $\sigma^{(i)}$ $(i = 1, 2, 3)$ are independent, which need to be fixed according to the available experimental data of fission mass distributions in actinide and transactinide nuclei.

For fitting the parameters in the three-Gaussian empirical formula, we collected as many available experimental data of fission mass distributions [17–21] as possible. In cases where experimental data are lacking, interpolation or extrapolation is employed. For ^{238}U, data for the mass distributions of fission fragments at different energies are available, so we can obtain the energy dependence of mass distribution of fission fragments through interpolation. However, these data are not available for other fissile nuclei. For these nuclei, we suppose that they have an energy dependence behavior similar to those of ^{238}U for lack of the corresponding theoretical study for these nuclei. This, of course, will introduce a considerable approximation. However, in the reaction considered in this work, the fission for excited ^{238}U is the most important among all fissile nuclei, and we expect that the approximation introduced in the energy dependence of the mass distribution of fission fragments will not severely damage the accuracy of the final results. In Figs. 2 and 3, we show some examples of calculated mass distributions of fission for different nuclei and for different excitation energies, and we compare these with experimental data. The curves and dots denote calculated results and data, respectively. From the figures, we can see that the empirical formula seems to successfully reproduce the available experimental data and can be used to calculate the mass distributions of actinide and transactinide fragments.

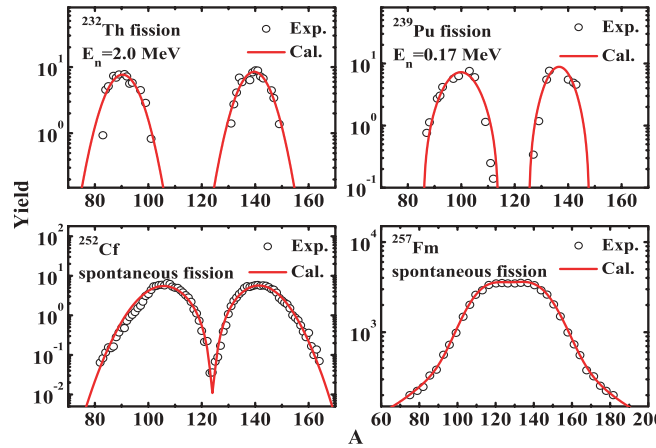

FIG. 2. (Color online) The mass distributions of fission products for ^{232}Th, ^{239}Pu, ^{252}Cf, and ^{257}Fm. The experimental data are taken from Refs. [21–24].

To choose the matching time t_S of two models properly, we investigate the decay process of the transiently formed composite systems of ^{238}U + ^{238}U at an energy of 7.0A MeV. Figure 4 shows the time dependence of the surviving probability of fragments with $Z \geqslant 110$. One can see from the figure that at about $t = 500$ fm/c, two nuclei reach a touching configuration. After about 1000 fm/c, the composite system begins to reseparate with a very large decay rate, and at about 3000 fm/c, almost all composite systems are separated. This process is described by the ImQMD model. The separated fragments continue to decay with a much lower decay rate. This process is expected to be described by the statistical decay model. Thus, we select the matching time of the two models to be 3000 fm/c. We tried other alternatives, such as $t_S = 4000$, 5000, and 6000 fm/c, and found that there is no change in the final results. In the ImQMD calculations, 500 events per impact parameter are performed.

III. THE DISTRIBUTION OF MASS, CHARGE, AND EXCITATION ENERGY IN PRIMARY FRAGMENTS

To study the final mass distribution of the reaction ^{238}U + ^{238}U, we first study the distribution of primary fragments, which are given at the end of ImQMD calculations. The charge, mass, and excitation energy distributions as well as the angular distribution of primary fragments are obtained by the ImQMD model calculations at time $t = 3000$ fm/c. The double differential cross section of a primary fragment with charge Z, mass A, excitation energy E, and scattering angle θ

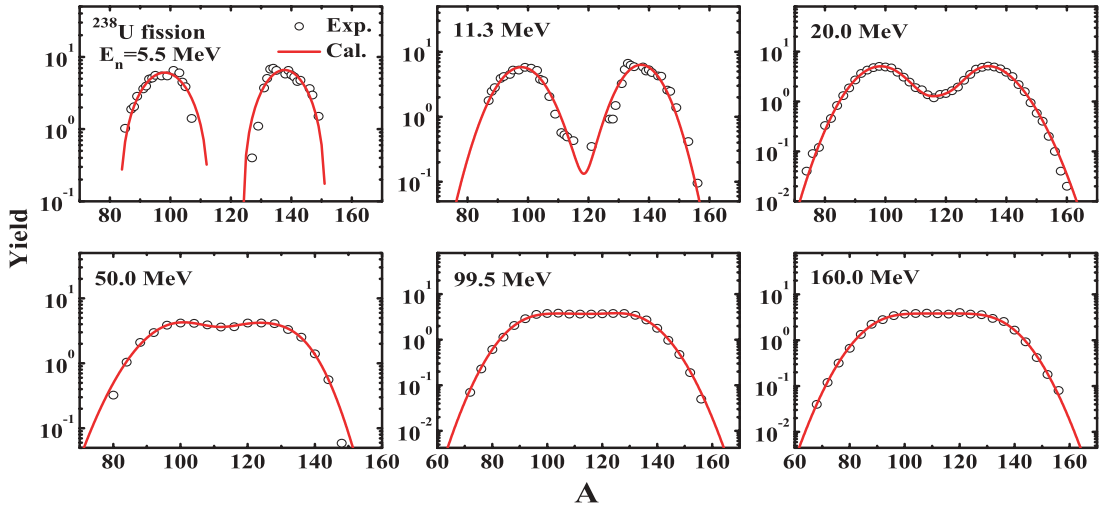

FIG. 3. (Color online) The mass distributions of fission products for ^{238}U at different excitation energies. The experimental data are taken from Ref. [21].

is given by

$$\frac{d^2\sigma_{\rm pri}(Z,A,E,\theta)}{d\theta dE} = \int_0^{b_{\max}} 2\pi b f(Z,A,E,\theta,b)db = \sum_{i=1}^{i_{\max}} 2\pi b_i \Delta b f_i(Z,A,E,\theta,b_i), \quad (10)$$

where $f_i(A,Z,E,\theta,b_i)$ is the probability of producing the primary fragments with charge Z, mass A, excitation energy E, and scattering angle θ under impact parameter b_i. The maximum impact parameter $b_{\max}$ is taken to be 14 fm because there is no inelastic scattering when $b > 14$ fm. The double differential cross section for primary fragments will be used as input in the second step for the calculations of final products to compare with the measurement. Let us first study the charge and mass distribution of primary fragments, which is the integration of double differential cross sections. Figures 5(a) and 5(b) show the charge and mass distribution of primary fragments ($A \geqslant 50$) for ^{238}U + ^{238}U at 7.0A MeV, respectively. A sharp peak indicates that uranium is present in both figures. The primary fragments on the left-hand side of the sharp peak stem from the reseparation of the composite system and fast fission products of actinide and transactinide fragments. The products on the right-hand side of the sharp peak correspond to transuranic nuclei.

The mass distributions of primary fragments at different impact parameters b are calculated to clarify the origin of the fragments with different mass regions. The results are shown in Fig. 6. Figures 6(a)–6(d) are for the impact parameters of 0–4, 5–7, 8–10, and 11–14 fm, respectively. In central collisions [see Fig. 6(a)], the mass number distribution of primary fragments extends to $A = 320$ with a big asymmetric hump around $A = 200$–260, which means that a large mass transfer between two uranium nuclei occurs in central collisions. In semicentral collisions [Fig. 6(b)], the mass distribution becomes narrower with a much shorter tail on the right-hand side. Two peaks appear in the mass distribution, with the larger one corresponding to uranium and the smaller one originating from ternary fission (or occasionally from quaternary fission) events in the reaction ^{238}U + ^{238}U. Clearly, in this case, a very deep inelastic reaction becomes the most important reaction mechanism. For the peripheral collisions [Figs. 6(c) and 6(d)], the mass distribution of primary fragments shows a symmetric peak with very little variance. The reaction mechanism for peripheral reactions is inelastic or elastic scattering between two uranium nuclei. To understand the reaction mechanism and the mass distribution of fragments evolving with impact parameters shown in Fig. 6, we present the average lifetime

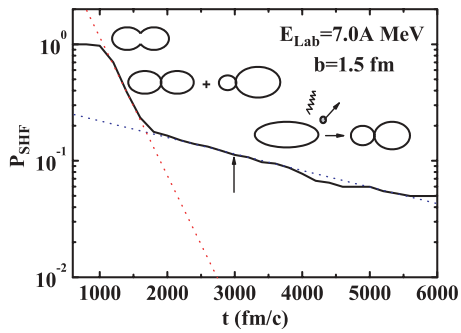

FIG. 4. (Color online) The time dependence of the surviving probability of superheavy fragments of $Z > 110$.

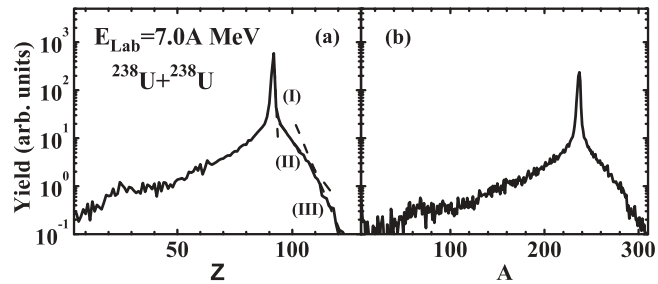

FIG. 5. (a) The charge and (b) the mass distribution of the primary fragments of ^{238}U + ^{238}U at 7.0A MeV.

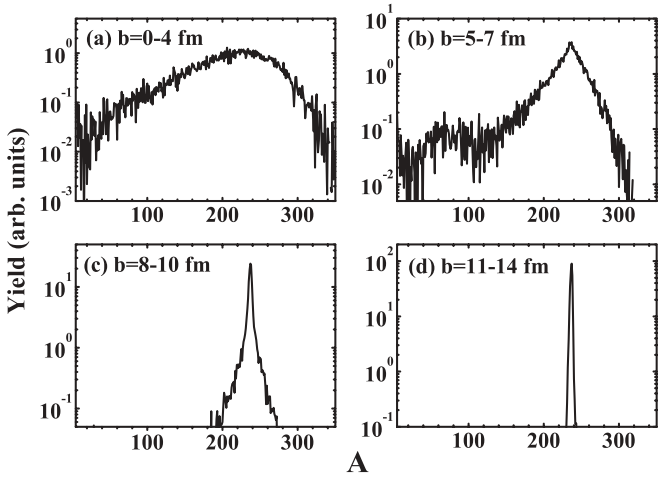

FIG. 6. The mass distributions of the primary fragments at different impact parameter regions.

of a transiently formed composite system for ^{238}U + ^{238}U at 7A MeV as a function of impact parameter in Fig. 7. From this figure, one can see that the lifetime of the composite system increases as impact parameter decreases. In central collisions, two uranium nuclei have a longer interaction time, with a stronger dissipation of collective motion, and thus there is stronger mass transfer between them than with larger impact parameter cases. Therefore, the transuranic primary fragments mainly come from the central and semicentral collisions.

Now we study the distribution of excitation energies of excited fragments. Figures 8 and 9 show the excitation energy distributions for fragments with $Z \geqslant 100$ and $90 \leqslant Z \leqslant 94$, respectively. Given that the fragments with $Z \geqslant 100$ come from the large mass transfer reactions, which only occur in the central and semicentral collisions, the results shown in Fig. 8 are only for impact parameters $b = 0$–4 and 5–7 fm. Figure 9 shows the results from deep inelastic scattering of ^{238}U + ^{238}U. One sees from both Figs. 8(a) and 9(a) that the primary fragments produced in central collisions are mostly highly excited; for those fragments the survival probability should be very low, but there is still a tail extending to a low exciting energy, which may have a certain but very small survival probability. However, for semicentral collisions [see Figs. 8(b) and 9(b)], the proportion of high-excitation-energy primary fragments decreases and the proportion of low-energy

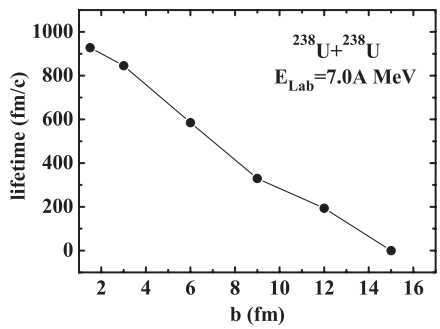

FIG. 7. The impact-parameter dependence of the average lifetime for the composite system of ^{238}U + ^{238}U at 7A MeV.

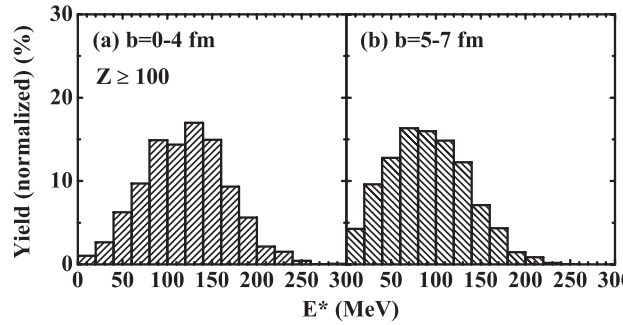

FIG. 8. The excitation energy distribution of the transuranic fragments with $Z \geqslant 100$ under the condition of impact parameters (a) $b \leqslant 4$ fm and (b) $b = 5$–7 fm.

primary fragments increases, and thus, it is expected that some of the fragments with $Z \geqslant 92$ can survive. In the peripheral collisions [see Figs. 9(c) and 9(d)], the excitation energies of primary fragments are much lower than with the central and semicentral cases, which is understandable.

IV. MASS DISTRIBUTION OF FINAL PRODUCTS

From the ImQMD model calculation, we obtain the distributions of charges, masses, and excitation energies for all primary fragments produced in ^{238}U + ^{238}U collisions. These primary fragments will de-excite through the emission of light particles or γ rays or through fission. The decay process and the final products are described by the statistical evaporation model (HIVAP code) incorporating the three-Gaussian fission model described in Sec. II. On the basis of this model, the mass distribution of final products for ^{238}U + ^{238}U at an incident energy of 7.0A MeV can be calculated. In Fig. 10, we show the calculated results of final products at four impact parameter regions of 0–4, 5–7, 8–10, and 11–14 fm. For central collisions [see Fig. 10(a)], the reseparation primary fragments of ^{238}U + ^{238}U systems carry high excitation energies, with the majority of them undergoing symmetric fission and thus

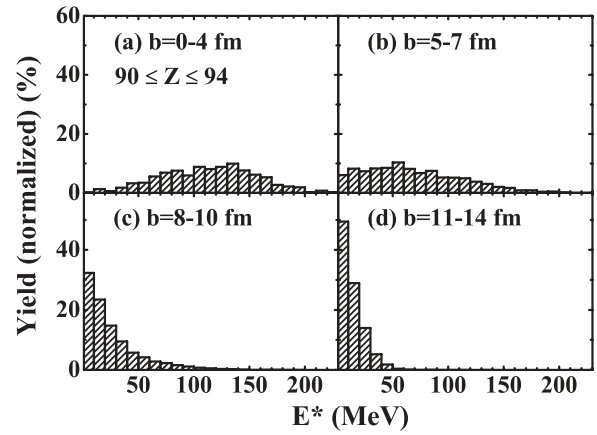

FIG. 9. The excitation energy distribution of the primary fragments around uranium ($90 \leqslant Z \leqslant 94$) for impact parameters (a) $b \leqslant 4$ fm, (b) $b = 5$–7 fm, (c) $b = 8$–10 fm, and (d) $b = 11$–14 fm.

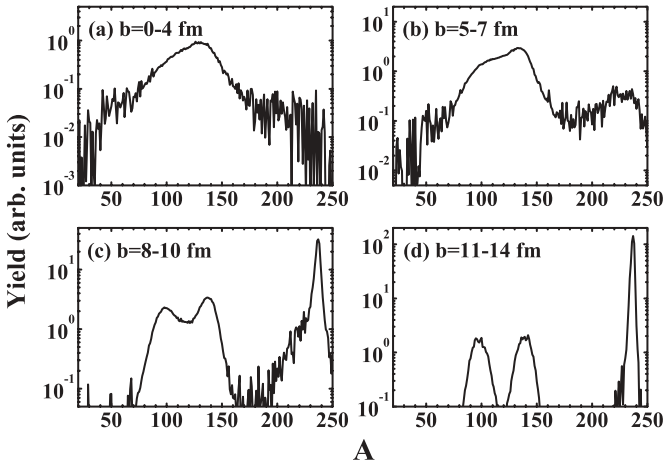

FIG. 10. The mass distribution of the products in ^{238}U + ^{238}U at different impact parameter regions.

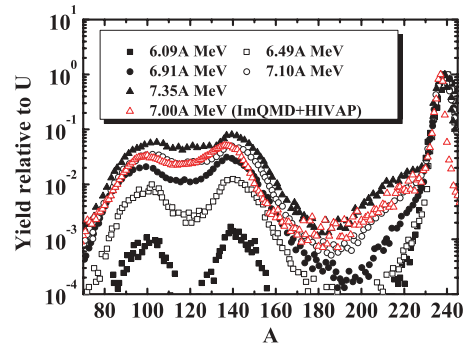

FIG. 11. (Color online) The mass distribution of the products of reaction ^{238}U + ^{238}U. The experimental data are taken from Ref. [9].

a single hump of mass yield is found at around mass number 120. The rest of the fragments that do not undergo fission will exhibit evaporation of particles, and their residues finally form a shoulder in the mass distribution around Pb, which is due to strong shell effects for those nuclei around Pb. The yields for transuranic fragments decrease rapidly as mass increases, which is due to the high excitation energy of primary fragments in central collisions, as seen from Fig. 8(a). Here, we should mention that the yields of the transuranic nuclei are not very certain because the fission barrier and the fission width for superheavy nuclei and the transuranic nuclei are largely uncertain. For semicentral collisions, that is, in the impact parameter region of 5–7 fm [see Fig. 10(b)], the excitation energies carried by primary fragments are much less than those in the central collisions, so a broad hump appears in the mass number region of $80 \leqslant A \leqslant 170$, which is the superposition of symmetric and asymmetric fission. Another small hump centered at uranium ($A \approx 230$) appears. The shallow valley between two humps means that the yields of nuclei around Pb are still considerable. Here, we notice that the yields of transuranic nuclei are relatively high compared with those in central collisions, which is due to the excitation energies of primary fragments being much lower than those in central collisions. For peripheral collisions [see Figs. 10(c) and 10(d)], elastic or inelastic scattering plays a dominant role and the behavior of low-energy fission of actinide nuclei is shown. The small shoulder around Pb seems to appear for impact parameters $b = 8$–10 fm [see Fig. 10(c)].

To perform a comparison with the experimental measurement, we must select a scattering angle to fit the angle cut in the experimental data, that is, only fragments with scattering angles of $56^\circ \leqslant \theta \leqslant 84^\circ$ and $96^\circ \leqslant \theta \leqslant 124^\circ$ in the center-of-mass frame are selected [9]. In the calculations, we assume that the scattering angle of the residue of the primary fragment that exhibits emission of light charged particles is the same as that of the fragment itself. This assumption is reasonable since the mass of the residue is much larger than that of the emitted light particles. For fragments from fission, we assume that the outgoing angle of one fragment is randomly distributed in the rest frame of the fissioning nucleus, and the outgoing angle of the other one is then obtained by momentum conservation. Finally, we obtain the mass distribution of the final products with the same scattering angle as that cut in the experiment. The results are shown by open triangles in Fig. 11. The experimental mass spectra from Ref. [9] are also indicated by solid squares, open squares, solid circles, open circles, and solid triangles for incident energies of 6.09, 6.49, 6.91, 7.10, and 7.35A MeV, respectively, in Fig. 11. From the figure, we find that the behavior of the calculated mass distribution at 7.0A MeV is generally in agreement with the data at the incident energy 7.10A MeV, except that the yields at the mass region from 170 to 210 are overestimated compared with the experimental data. The most important features of mass distribution are considered to be the following: (1) A dominant peak around uranium is observed; this can be attributed to the contribution of the reactions with large impact parameters, as seen in Fig. 10. (2) A steep decreasing yield above U with increasing mass number appears. The products at this mass region stem from large mass transfer in small-impact-parameter reactions. (3) A small shoulder can be seen in the distribution of the products around Pb, compared with the products with a mass near and smaller than uranium for which the yields decrease exponentially as mass decreases. The appearance of the small shoulder is due to the very high fission barrier around Pb. The central and semicentral collisions, and even reactions with $b = 8$–10 fm, contribute to the shoulder in the region around Pb. (4) In the region below $A \approx 190$, a double hump distribution is observed. This is clearly due to the fission of actinide and transuranic nuclei, which results in the superposition of symmetric and asymmetric fission.

V. SUMMARY

In this paper, we apply the microscopic transport model, namely the ImQMD model incorporating the statistical decay model and empirical three-Gaussian fission model, to study the reaction mechanism and the mass distribution of products in the reaction ^{238}U + ^{238}U at an incident energy of 7.0A MeV. The mass, charge, and excitation energy distributions of primary fragments are calculated within the ImQMD model, and the de-excitation process of those primary fragments is

studied using the statistical-evaporation model (HIVAP code). The impact-parameter dependence of the mass distribution of primary fragments and final products are analyzed, from which the origin of products at different mass regions can be understood. Finally, the mass distribution of final products in $^{238}U + ^{238}U$ collisions with the scattering angle cut is calculated for the first time and compared with recent experimental data. The main features of experimental mass distribution are reproduced, which are as follows: (1) A dominant peak around the uranium nuclei is observed; this corresponds to elastic and quasielastic reaction products. (2) The yields of the transuranic nuclei decrease rapidly with increasing mass A. (3) A small shoulder can be seen in the mass distribution of the products around Pb on the background of products whose yields decrease exponentially with their mass deviating from that of uranium. These products are the residues of primary fragments surviving from multiple-particle evaporation. (4) In the region below $A \approx 200$, a double-hump mass distribution is observed, which is due to the fission products from superposition of symmetric and asymmetric fission that mainly arise from the fission of nuclei around uranium and transuranic fragments at high and low excitation energies. The main discrepancies of our calculated results from the experimental data are an overestimation of mass yields in the region of 170–200 and an underestimation of the mass yields of transuranic nuclei, which mainly arise from the calculation of fission mass distribution for actinide and transuranic nuclei and fission width at high excitation energies. Further study is underway.

ACKNOWLEDGMENTS

This work is supported by grants from the National Natural Science Foundation of China, Nos. 10675172 and 10875031, and from the National Basic Research Program of China, No. 2007CB209900.

[1] K. D. Hildenbrand, H. Freiesleben, F. Pühlhofer, W. F. W. Schneider, R. Bock, D. V. Harrach, and H. J. Specht, Phys. Rev. Lett. **39**, 1065 (1977).
[2] M. Schadel *et al.*, Phys. Rev. Lett. **41**, 469 (1978).
[3] H. Freiesleben *et al.*, Z. Phys. A **292**, 171 (1979).
[4] V. I. Zagrebaev and W. Greiner, J. Phys. G **34**, 1 (2007).
[5] V. I. Zagrebaev, Yu. Ts. Oganessian, M. G. Itkis, and W. Greiner, Phys. Rev. C **73**, 031602(R) (2006).
[6] N. Wang *et al.*, Mod. Phys. Lett. A **20**, 2619 (2005).
[7] J. Tian, X. Wu, K. Zhao, Y. Zhang, and Z. Li, Phys. Rev. C **77**, 064603 (2008).
[8] C. Golabek and C. Simenel, Phys. Rev. Lett. **103**, 042701 (2009); C. Simenel, B. Avez, and C. Golabek, arXiv:0904.2653V1 [nucl-th].
[9] C. Golabek *et al.*, Int. J. Mod. Phys. E **17**, 2235 (2008).
[10] S. Heinz *et al.*, GSI Scientific Report 2006, p. 136 (2007); S. Heinz *et al.*, GSI Scientific Report 2007, p. 147 (2008).
[11] N. Wang, Z. Li, and X. Wu, Phys. Rev. C **65**, 064608 (2002).
[12] N. Wang, Z. Li, X. Wu, J. Tian, Y. X. Zhang, and M. Liu, Phys. Rev. C **69**, 034608 (2004).
[13] J. Cugnon, D. L'Hôte, and J. Vandermeulen, Nucl. Instrum. Methods Phys. Res. B **111**, 215 (1996).
[14] Y. Zhang and Z. Li, Phys. Rev. C **74**, 014602 (2006).
[15] Q. Li and Z. Li, Phys. Rev. C **64**, 064612 (2001).
[16] W. Reisdorf *et al.*, Nucl. Phys. **A444**, 154 (1985).
[17] E. F. Neuzil and A. W. Fairhall, Phys. Rev. **129**, 2705 (1963).
[18] J. Benlliure *et al.*, Nucl. Phys. **A628**, 458 (1998).
[19] K.-H. Schmidt *et al.*, Nucl. Phys. **A665**, 221 (2000).
[20] D. M. Gorodisskiy *et al.*, Phys. Lett. **B548**, 45 (2002).
[21] IAEA, *Fission Product Yield Data for the Transmutation of Minor Actinide Nuclear Waste* (International Atomic Energy Agency, Vienna, 2008).
[22] L. E. Glendenin, J. E. Gindler, I. Ahmad, D. J. Henderson, and J. W. Meadows, Phys. Rev. C **22**, 152 (1980).
[23] H. W. Schmitt, W. E. Kiker, and C. W. Williams, Phys. Rev. **137**, B837 (1965).
[24] W. John *et al.*, Phys. Rev. Lett. **27**, 45 (1971).